Baffle orientation and geometry effects on turbulent heat transfer of a constant property incompressible fluid flow inside a rectangular channel

Received 1 December 2018
Revised 3 March 2019
Accepted 12 March 2019

Younes Menni
Unit of Research on Materials and Renewable Energies, Department of Physics, Faculty of Sciences, Abou Bekr Belkaid University, Tlemcen, Algeria

A. Chamkha
Mechanical Engineering Department, Prince Sultan Endowment for Energy and Environment, Prince Mohammad Bin Fahd University, Al-Khobar, Saudi Arabia, and RAK Research and Innovation Center, American University of Ras Al Khaimah, United Arab Emirates, Saudi Arabia

Chafika Zidani
Department of Physics, Research Unit of Materials and Renewable Energies – URMER – Abou Bekr Belkaid University of Tlemcen, Tlemcen, Algeria, and

Boumédiène Benyoucef
Unit of Research on Materials and Renewable Energies, Department of Physics, Faculty of Sciences, Abou Bekr Belkaid University, Tlemcen, Algeria

Abstract

Purpose – A computational fluid dynamics (CFD) analysis has been carried out on the aerodynamic and thermal behavior of an incompressible Newtonian fluid having a constant property and flowing turbulently through a two-dimensional horizontal high-performance heat transfer channel with a rectangular cross section. The top surface of the channel was kept at a constant temperature, while it was made sure to maintain the adiabatic condition of the bottom surface. Two obstacles, with different shapes, i.e. flat rectangular and V-shaped, were inserted into the channel; they were fixed to the top and bottom surfaces of the channel in a periodically staggered manner to force vortices to improve the mixing and consequently the heat transfer. The first fin-type obstacle is placed on the heated top channel surface, and the second baffle-type one is placed on the insulated bottom surface. Five different obstacle situations were considered in this study, which are referred as cases FF (flat fin and flat baffle), FVD (flat fin and V-downstream baffle), FVU (flat fin and V-upstream baffle), VVD (V-downstream fin and V-downstream baffle) and VVU (V-Upstream fin and V-upstream baffle).

Design/methodology/approach – The flow model is governed by Reynolds-averaged Navier–Stokes equations with the k-epsilon turbulence model and the energy equation. These governing equations are discretized by the finite volume method, in two dimensions, using the commercial CFD software FLUENT software with the Semi Implicit Method for Pressure Linked Equations (SIMPLE) algorithm for handling the pressure-velocity coupling. Air is the test fluid with the flow rate in terms of Reynolds numbers ranging from 12,000 to 32,000.

Findings – Important deformations and large recirculation regions were observed in the flow field. A vortex causes a rotary motion inside the flow field, which enhances the mixing by bringing the packets of fluid from the near-wall region of the channel to the bulk and the other way around. The largest value of the axial variations of

International Journal of Numerical Methods for Heat & Fluid Flow

0961-5539
DOI 10.1108/HFF-12-2018-0718

the Nusselt number and skin friction coefficient is found in the region facing the baffle, while the smallest value is in the region near the fin, for all cases. The thermal enhancement factor (TEF) was also introduced and discussed to assess the performance of the channel for various obstacle situations. It is found that the TEF values are 1.273-1.368, 1.377-1.573, 1.444-1.833, 1.398-1.565 and 1.348-1.592 for FF, FVD, FVU, VVD and VVU respectively, depending on the *Re* values. In all cases, the TEF was found to be much larger than unity; its maximum value was around 1.833 for FVU at the highest Reynolds number. Therefore, the FVU may be considered as the best geometrical configuration when using the obstacles to improve the heat transfer efficiency inside the channel.

Originality/value – This study can be a real application in the field of shell-and-tube heat exchangers and flat plate solar air collectors.

Keywords Aerodynamics, Computational fluid dynamics, Friction loss, Finite volumes, Thermal enhancement, Numerical simulation, CFD

Paper type Research paper

Nomenclature

C_f = skin friction coefficient;
D_h = aeraulic diameter of channel (m);
f = friction factor;
H = channel height (m);
h = obstacle height (m);
h_x = local heat transfer coefficient ($W/m^2 K$);
k = turbulent kinetic energy (m^2/s^2);
k_f = fluid thermal conductivity (W/m K);
L = channel length (m);
L_{in} = distance upstream of the first obstacle (m);
L_{out} = distance downstream of the second obstacle (m);
Nu = average Nusselt number;
Nu_x = local Nusselt number;
P = pressure (Pa);
P_{atm} = atmospheric pressure (Pa);
Pi = separation distance between obstacles (m);
Pr = Prandtl number;
Re = Reynolds number;
t = obstacle thickness (m);
T = temperature (K);
T_{in} = inlet temperature (K);
T_w = wall temperature (K);
TI_{in} = inlet turbulence intensity (%);
U_{in} = inlet velocity (m/s);
$\overline{U}$ = mean air velocity (m/s);
u = axial component of velocity (m/s);
v = transverse component of velocity (m/s);
x = axial coordinate (m); and
y = transverse coordinate (m).

Greek symbols

ϕ = transported scalar;
ϵ = turbulent energy dissipation (m^2/s^3);
Γ_ϕ = turbulent diffusion coefficient;
S_ϕ = source term;

ρ = fluid density (kg/m^3);
ΔP = pressure drop (Pa);
τ_w = wall shear stress (Pa);
α = flow attack angle of V-baffle (degree);
TEF = thermal enhancement factor;
μ = molecular viscosity (kg/m s);
μ_e = effective viscosity (kg/m s);
μ_l = laminar viscosity (kg/m s);
μ_t = eddy viscosity (kg/m s);
σ_k = turbulent model constant for k;
σ_ε = turbulent model constant for ε;
σ_T = turbulent model constant for T;
$C_{1\varepsilon}$ = constant used in the standard k-ε model; and
$C_{2\varepsilon}$ = constant used in the standard k-ε model.

Subscript

atm = atmospheric;
e = effective;
f = fluid;
in = inlet;
l = laminar;
out = outlet;
t = turbulent;
w = wall; and
x = local.

Abbreviations

CFD = computational fluid dynamics;
FF = flat fin and flat baffle;
FVD = flat fin and v-downstream baffle;
FVM = finite volume method;
FVU = flat fin and v-upstream baffle;
QUICK = quadratic upstream interpolation for convective kinetics;
RANS = Reynolds-averaged Navier–stokes;
SIMPLE = semi implicit method for pressure linked equations;
SOU = second-order upwind;
TEF = thermal enhancement factor;
VVD = V-downstream fin and V-downstream baffle; and
VVU = V-upstream fin and V-upstream baffle.

1. Introduction

One of the most effective passive techniques for improving the convective heat transfer rate in smooth air channels, such as "heating, cooling or solar" ducts (Verma and Prasad, 2000; Aharwal *et al.*, 2008; Mehryan *et al.*, 2018; Tahmasebi *et al.*, 2018; Ghalambaz *et al.*, 2014a, 2014b; Ghalambaz and Noghrehabadi, 2014; Behseresht *et al.*, 2014; Noghrehabadi *et al.*, 2013) at "low, moderate or high" Reynolds numbers (Hwang and Lin, 1999; Endres and Möller, 2001; Maurer *et al.*, 2007; Mansour *et al.*, 2016; Ahmed *et al.*, 2013; EL-Kabeir *et al.*, 2007; Rashad, 2008; Rashad *et al.*, 2011; Shuja *et al.*, 2010), is the use of "attached, semiattached or detached" (Liou and Wang, 1995; Liu and Wang, 2011; Yongsiri *et al.*, 2014),

"transverse or longitudinal" (Ben Slama, 2007; Pirouz *et al.*, 2011), "parallel, orthogonal or inclined" (Demartini *et al.*, 2004; Won *et al.*, 2004; Nasiruddin and Siddiqui, 2007), "solid, perforated or porous" (Ko and Anand, 2003; Sahel *et al.*, 2016) and "simple, corrugated or shaped" (Taslim and Li, 1996; Lei *et al.*, 2008; Zhou and Ye, 2012; Jedsadaratanachai and Boonloi, 2014; Ünalan *et al.*, 2007) type obstacles, known as "vortex generators" (Fiebig *et al.*, 1991) "elements" (Habib *et al.*, 1988), "turbulators" (Han and Park, 1988), "deflectors" (Demartini *et al.*, 2004), or "disturbance promoters" (Han *et al.*, 1985), such as "ribs" (Karwa, 2003; Nguyen *et al.*, 2017), "fins" (Kelkar and Patankar, 1987; Sheremet and Chinnasamy, 2018; Yang *et al.*, 2012; Kahalerras and Targui, 2008) or "baffles" (Berner *et al.*, 1984; Ho and Ramaswamy, 1995; Armaghani *et al.*, 2018), placed on or near the insulated and/or heated channel walls (Dutta and Hossain, 2005; Tanda, 2011) with in-line or staggered manners (Tamna *et al.*, 2014). This is because the obstacle helps to interrupt the hydrodynamic and thermal boundary layers and to induce a vortex downstream (Sripattanapipat and Promvonge, 2009). The vortex creates a rotating motion within the flow stream, which causes a rapid transfer of fluid parcels to and from the heat transfer surface (Nasiruddin and Siddiqui, 2007). This method of heat transfer enhancement is commonly used in various practical engineering and industrial applications such as heat exchangers, solar air collectors, gas turbine cooling systems, nuclear reactors and electronic packages, so the literature on this topic is widely apparent (Sripattanapipat and Promvonge, 2009).

The present work focuses on the study of an interesting topic from different points of view, i.e. theoretical, practical and numerical modeling. This study aims to improve the heat transfer within thermal devices such as heat exchangers, solar air collectors and other electronic equipment; these thermal devices play a major role in the industry these days. This work consists of a computational fluid dynamics (CFD) analysis of a turbulent forced-convection constant property Newtonian fluid flow in the presence of two differently shaped solid-type obstacles, i.e. flat rectangular and/or V-shaped, arranged in an overlapping manner, in a horizontal channel of rectangular section. This channel section, due to of their specific geometry, accelerates the turbulence and improves the heat transfer. To perform a detailed study of the aerodynamic and heat transfer characteristics within this type of channel, the finite volume approach for a steady-state, incompressible and two-dimensional flow is used. The effects of obstacle geometries and orientations, as well as flow rates, are analyzed. A detailed description of turbulent heat transfer and flow behaviors around the obstacles was presented. In particular, contour plots of velocity and pressure fields, axial velocity profiles, local and average heat transfer coefficients, skin friction loss evaluations and thermal enhancement factors were obtained at constant wall temperature condition along the heated top channel walls for various Reynolds number values of 12,000-32,000.

2. Physical model and mathematical modeling

The CFD simulations were conducted in a two-dimensional horizontal domain, which represents a rectangular cross section channel of 0.554 m length, 0.146 m height and 0.167 m aeraulic diameter. A constant surface temperature is applied from the upper wall, but the surface lower is maintained at an adiabatic condition. Two obstacles, with different shapes, i.e. flat rectangular and/or 45° V-shaped, were inserted into the channel; they were fixed to the top and bottom walls of the channel in a periodically staggered manner to develop vortices to improve the mixing and thus the heat transfer. The first fin-type obstacle is placed on the heated top surface at a distance of L_{in} = 0.218 m from the upstream end of the channel, and the second baffle-type one is placed on the insulated bottom surface at a distance of L_{out} = 0.174 m from the downstream end of this same channel. The obstacle spacing and thickness are fixed at t = 0.01 m and Pi = 0.142 m, respectively. For both the fin

and the baffle, the transverse distance between the upper edge of the obstacle and the wall was kept constant at 0.08 m. This corresponds to the area reduction of 54.79 per cent at the obstacle edge. These dimensions were based on the experimental study of Demartini *et al.* (2004). The effects obstacle shape and disposition on the heat transfer improvement are investigated in detail. Five different obstacle situations are proposed, i.e. flat fin and flat baffle [FF case, see Figure 1(a)], flat fin and V-downstream baffle [FVD case, Figure 1(b)], flat fin and V-upstream baffle [FVU, see Figure 1(c)], V-downstream fin and V-downstream baffle [VVD case, see Figure 1(d)], and V-upstream fin and V-upstream baffle [VVU case, see Figure 1(e)]. Air, whose Prandtl number (Pr) is 0.71, is the working fluid used, and the Reynolds numbers considered range from 12,000 to 32,000.

The following assumptions were made to develop the numerical model for the fluid flow and heat transfer in the computational domain under the following conditions:

- Steady state, two-dimensional, turbulent, incompressible Newtonian fluid flow is considered.
- The physical properties of the fluid and solid are kept constant.
- Body forces, viscous dissipation and radiation heat transfer are not considered.

Based on the above assumptions, the channel flow model is governed by the Reynolds-averaged Navier–Stokes (RANS) equations with the standard k-ε turbulence model, developed by Launder and Spalding (1974), and the energy equation. These governing equations can then be written in the conservative form as:

$$\frac{\partial}{\partial x}(\rho u \phi) + \frac{\partial}{\partial y}(\rho v \phi) = \frac{\partial}{\partial x}\left[\Gamma_\phi \frac{\partial \phi}{\partial x}\right] + \frac{\partial}{\partial y}\left[\Gamma_\phi \frac{\partial \phi}{\partial y}\right] + S_\phi \tag{1}$$

in which ϕ is a variable used to represent quantities such as velocity components u, v, turbulent kinetic energy k, or turbulent energy dissipation rate ε and temperature T, while the diffusion coefficient Γ_ϕ and the source term S_ϕ have specific values for the different conservation equations using the standard k-ε turbulence model as:

Continuity equation:

$$\phi = 1 \tag{2}$$

$$\Gamma_\phi = 0 \tag{3}$$

$$S_\phi = 0 \tag{4}$$

Momentum equation in x-direction:

$$\phi = u \tag{5}$$

$$\Gamma_\phi = \mu_e \tag{6}$$

$$S_\phi = \frac{\partial P}{\partial x} + \frac{\partial}{\partial x}\left[\mu_e\left(\frac{\partial u}{\partial x}\right)\right] + \frac{\partial}{\partial y}\left[\mu_e\left(\frac{\partial v}{\partial x}\right)\right] \tag{7}$$

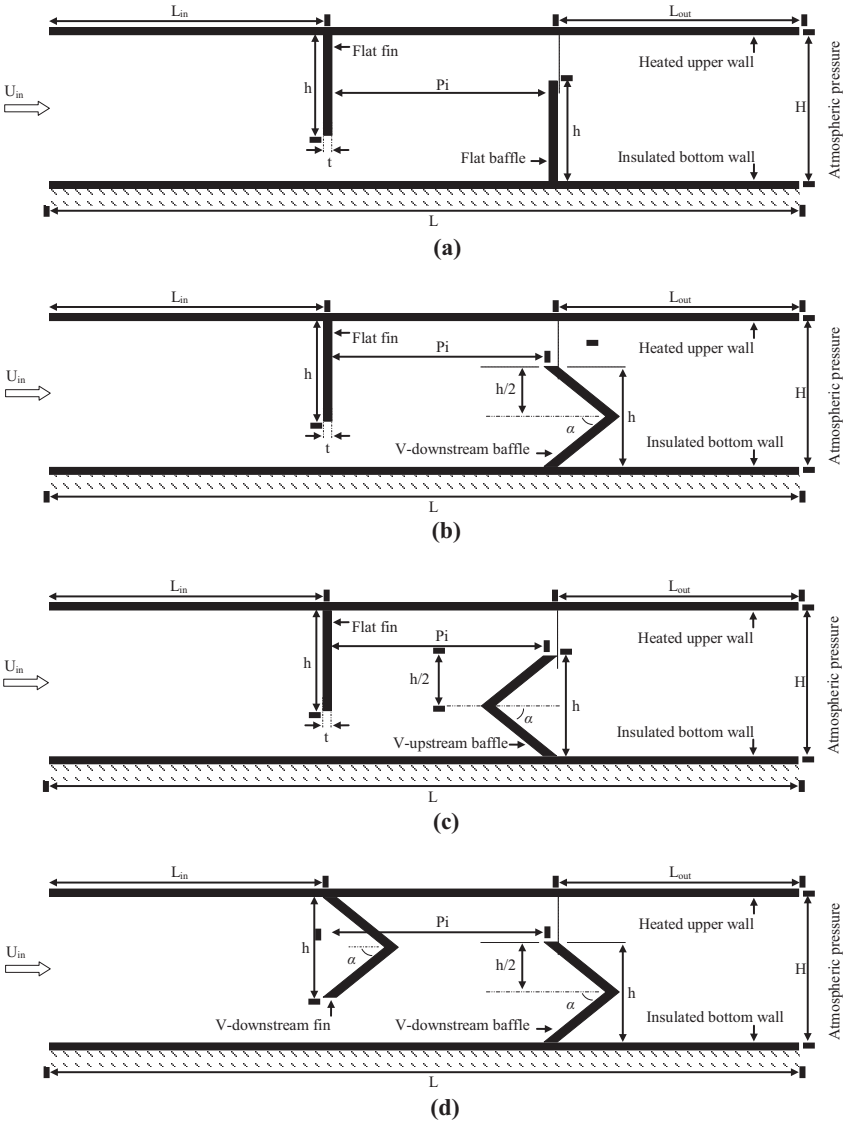

Figure 1.
The two-dimensional physical model that represents a rectangular channel for various obstacle situations

Notes: (a) Case FF with flat fin and flat baffle; (b) case FVD with flat fin and 45° V-downstream baffle; (c) case FVU with flat fin and 45° V-upstream baffle; (d) case VVD with 45° V-downstream fin and 45° V-downstream baffle; (e) case VVU with 45° V-upstream fin and 45° V-upstream baffle

Momentum equation in y-direction:

$$\phi = v \tag{8}$$

$$\Gamma_\phi = \mu_e \tag{9}$$

$$S_\phi = \frac{\partial P}{\partial y} + \frac{\partial}{\partial x}\left[\mu_e\left(\frac{\partial u}{\partial y}\right)\right] + \frac{\partial}{\partial y}\left[\mu_e\left(\frac{\partial v}{\partial y}\right)\right] \tag{10}$$

Energy equation:

$$\phi = T \tag{11}$$

$$\Gamma_\phi = \frac{\mu_e}{\sigma_T} \tag{12}$$

$$S_\phi = 0 \tag{13}$$

k-turbulent kinetic energy equation:

$$\phi = k \tag{14}$$

$$\Gamma_\phi = \mu_l + \frac{\mu_t}{\sigma_k} \tag{15}$$

$$S_\phi = -\rho\varepsilon + G_k \tag{16}$$

ε-turbulent dissipation rate equation:

$$\phi = \varepsilon \tag{17}$$

$$\Gamma_\phi = \mu_l + \frac{\mu_t}{\sigma_\varepsilon} \tag{18}$$

$$S_\phi = \frac{\varepsilon}{k}(C_{1\varepsilon}G_k - C_{2\varepsilon}\rho\varepsilon) \tag{19}$$

where:

$$\mu_{eff} = \mu_l + \mu_t \tag{20}$$

and G_k is the production rate of the kinetic energy due to the energy transfer from the mean flow to turbulence given by:

$$G_k = \mu_t \left\{ 2\left[\left(\frac{\partial u}{\partial x}\right)^2 + \left(\frac{\partial v}{\partial y}\right)^2 \right] + \left(\frac{\partial u}{\partial y} + \frac{\partial v}{\partial x}\right)^2 \right\} \quad (21)$$

where C_μ, $C_{1\varepsilon}$, $C_{2\varepsilon}$, σ_k, σ_ε and σ_T are the turbulence model constants. Their standard values, which are used in the present work, are described in Launder and Spalding (1974).

The limits of the computational domain are also illustrated in Figure 1.

A uniform one-dimensional velocity profile (U_{in})was used as the aeraulic boundary condition at the intake of the computational domain (Demartini *et al.*, 2004; Nasiruddin and Siddiqui, 2007). The temperature (T_{in}) of the working fluid was set equal to 300 K at the inlet of the channel (Nasiruddin and Siddiqui, 2007). A turbulence intensity (TI_{in}) equal to 2 per cent was selected for the intake height (Demartini *et al.*, 2004). The thermal boundary condition consisted of the constant temperature (T_w) of 375 K (Nasiruddin and Siddiqui, 2007), which was applied to the upper wall of the computational domain. The bottom surface of the computational domain was taken as adiabatic. Moreover, it was decided to impose the no-slip and impermeability boundary conditions at all the solid walls (Demartini *et al.*, 2004). Note that the atmospheric pressure (P_{atm}) is prescribed at the channel outlet (Demartini *et al.*, 2004).

The Reynolds number is a dimensionless parameter that is defined as follows (Demartini *et al.*, 2004):

$$\mathrm{Re} = \rho U_{in} D_h / \mu \quad (22)$$

Here, the quantities ρ, μ and U_{in} are the density, dynamic viscosity and inlet velocity of the fluid, respectively, while D_h, equal to 0.167 m, is the hydraulic diameter of the rectangular channel.

The skin friction coefficient (C_f) is expressed as (Sripattanapipat and Promvonge, 2009):

$$C_f = \frac{\tau_w}{\frac{1}{2}\rho \overline{U}^2} \quad (23)$$

The friction factor (f) is calculated by considering the pressure drop (ΔP) across the channel length (L) as (Sripattanapipat and Promvonge, 2009):

$$f = \frac{(\Delta P/L) D_h}{\frac{1}{2}\rho \overline{U}^2} \quad (24)$$

Note that τ_w is the wall shear stress, and $\overline{U}$ is the mean velocity of the airflow in the channel.

The local Nusselt number can be calculated using the expression (Sahel *et al.*, 2016):

$$Nu_x = \frac{h_x D_h}{k_f} \quad (25)$$

where h_x is the local heat transfer coefficient based on the bulk temperature and k_f is the thermal conductivity of air.

The average Nusselt number (*Nu*) can be determined using (Sahel *et al.*, 2016):

$$Nu = \frac{1}{L}\int Nu_x \partial x \quad (26)$$

The following expression represents the thermal enhancement factor (TEF) (Sahel *et al.*, 2016):

$$TEF = (Nu/Nu_0)/(f/f_0)^{1/3} \quad (27)$$

The Dittus–Boelter and Petukhov correlations can be used to normalize the average Nusselt number and friction factor, respectively. The quantities Nu_0 and f_0 are the average Nusselt number and the friction factor of the smooth channel, respectively.

The Dittus and Boelter correlation has the form (Dittus and Boelter, 1930):

$$Nu_0 = 0.023\mathrm{Re}^{0.8}\mathrm{Pr}^{0.4} \quad \text{for} \quad \mathrm{Re} \geq 10^4 \quad (28)$$

The Petukhov correlation has the form (Petukhov, 1970):

$$f_0 = (0.79\ln\mathrm{Re} - 1.64)^{-2} \quad \text{for} \quad 3 \times 10^3 \leq \mathrm{Re} \leq 5 \times 10^6 \quad (29)$$

3. Numerical modeling and validation

The fluid flow and temperature fields were simulated using the commercial CFD software FLUENT. The same package included a preprocessor GAMBIT which was utilized to create the mesh needed for the solver. A two-dimensional non-uniform grid was used. Figure 2 illustrates the refined mesh at all solid boundaries for all cases investigated. This refinement is required if one wants to resolve the important velocity and temperature gradients in the region under consideration. The mesh is uniform for the regions that are far away from the walls, as depicted in Figure 2. RANS equations, along with the standard k-ϵ turbulence model (Launder and Spalding, 1974) and the energy equation, are used to control the channel flow model. These equations were discretized by the finite volume method (FVM) (Patankar, 1980), by means of a two-dimensional formulation, using the SIMPLE-pressure-velocity coupling algorithm (Patankar, 1980). With regard to the flow characteristics, the interpolation QUICK-scheme (Leonard and Mokhtari, 1990) was applied, and a second-order upwind scheme (Patankar, 1980) was used for the pressure terms. Moreover, various grid

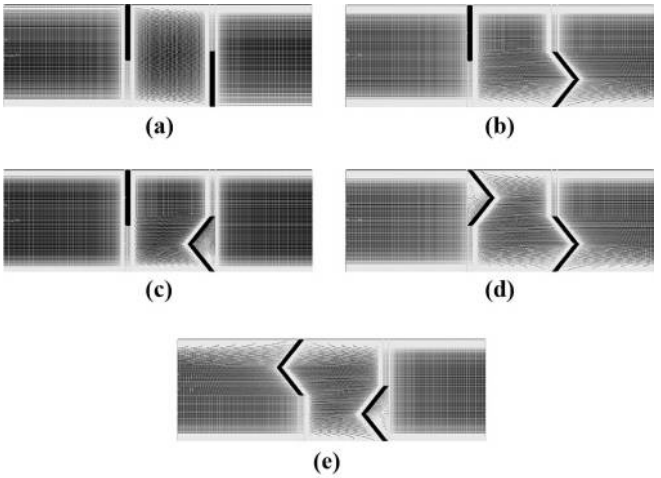

Notes: (a) FF; (b) FVD; (c) FVU; (d) VVD; (e) VVU cases

Figure 2.
Mesh resolution with refinements near the solid boundary for various obstacle situations

systems were tested to analyze the effect of the grid size on the numerical solution, and a mesh system of 245 × 95 cells was chosen in x and y directions, respectively.

Then, the results obtained from our CFD analysis using the FLUENT are validated through comparison with the numerical and experimental results reported by Demartini *et al.* (2004), which are available in the literature. For this reason, the same conditions are kept. Figure 3(a) and (b) gives the validation plots of the pressure coefficient (C_p) and the axial velocity (u) for Re = 8.73×10^4, respectively. Both the numerical and experimental profiles of C_p and u are measured along the channel height at locations $x = 0.223$ and $x = 0.525$ m from entrance, respectively. As observed in these figures, the comparison shows

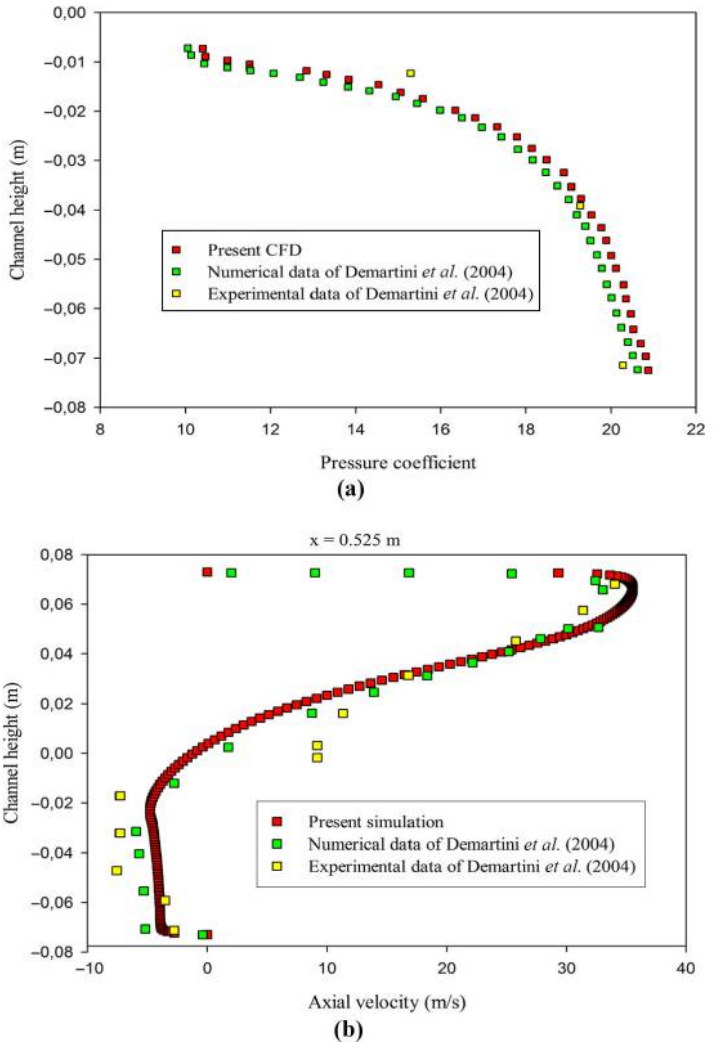

Figure 3.
Validation plots of (a) pressure coefficient profiles at $x = 0.223$ m and (b) axial velocity profiles at $x = 0.525$ m, with reported data (Demartini *et al.*, 2004) for Re = 8.73×10^4

that there is a qualitative agreement and a very good concordance between the different results.

The current CFD analysis results on heat and friction loss are also validated by comparing the predicted Nusselt number (Nu_0) and friction factor (f_0) with the results obtained from the well-known steady-state flow correlations of Dittus and Boelter (1930) and Petukhov (1970), respectively, for the turbulent forced-convection smooth channel flow. The Nu_0 and f_0 obtained from the present smooth channel and the correlations of equations (28) and (29) at Reynolds numbers from 1.2×10^4 to 3.2×10^4 are plotted in Figure 4(a) and (b), respectively. As it can be shown in Figure 4, the present smooth channel results agree well

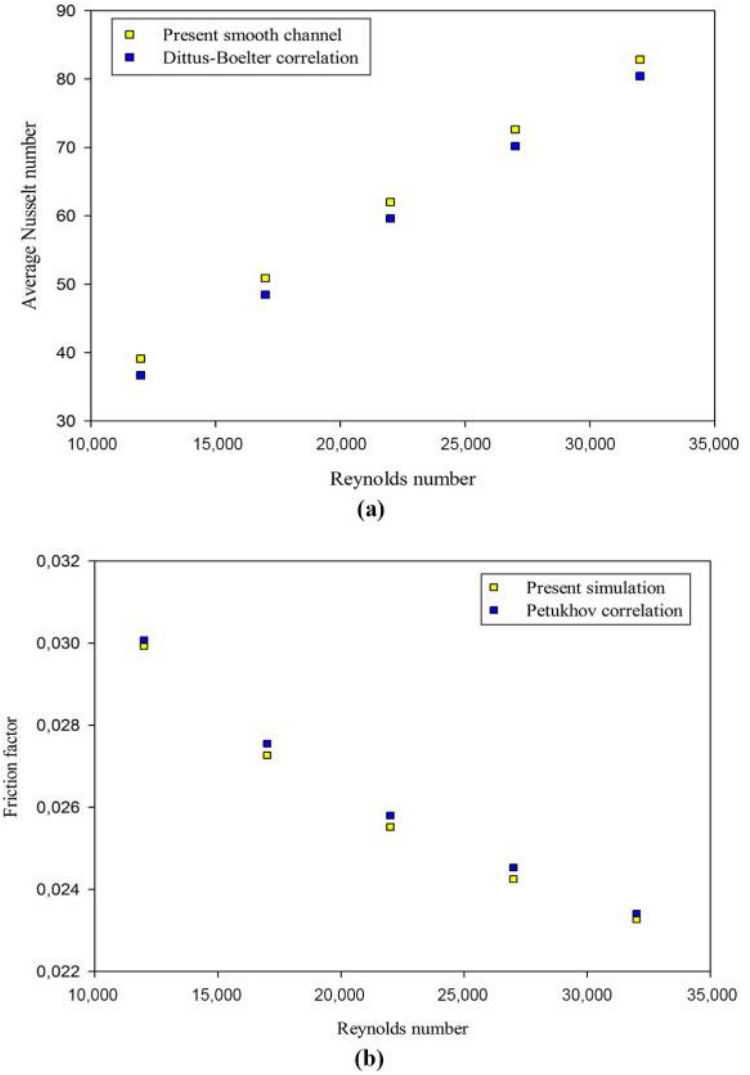

Figure 4.
Verification of (a) Nusselt number and (b) friction factor of smooth channel

with the available correlations with ±3.5 per cent in comparison with Dittus–Boelter correlation for the Nu_0 and ±1.15 per cent in comparison with Petukhov correlation for f_0.

4. Results and discussion

4.1 Flow structure and temperature field

The effect of obstacle shape and orientation parameters on the field of the near surface airflow is shown in Figure 5(a)-(e). The contour plots as described in this figure present the stream function for different treated cases (FF, FVD, FVU, VVD and VVU) at Re = 12,000. It is clearly noted that the fluid velocity values are almost negligible near the two obstacles, particularly in the downstream areas; this is caused by the presence of the recirculation

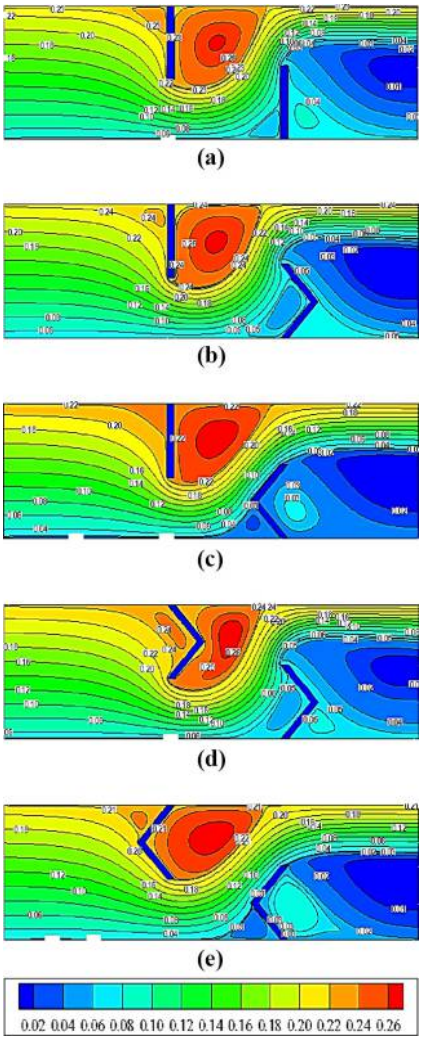

Figure 5.
Stream function contours in kg/s for (a) FF-, (b) FVD-, (c) FVU-, (d) VVD- and (e) VVU-type obstacles at Re = 12,000

zones. Far from these regions, the current lines become parallel, which leads to the progressive development of the flow.

It is also worth noticing that the axial velocity increases in the region extending from the end of each obstacle to the wall of the channel. This rise in velocity is caused by the presence of the obstacles and also by the presence of recycling; hence, an abrupt change in the direction of the flow comes out. One can also notice that the largest velocity values are found near the hot top wall of the channel. The flow starts accelerating just after the second obstacle to finally reach values of the order of 437.167, 456.626, 331.750, 455.796 and 323.214 per cent of the intake velocity, for using FF, FVD, FVU, VVD and VVU obstacles, respectively, as shown Figure 6(a)-(e).

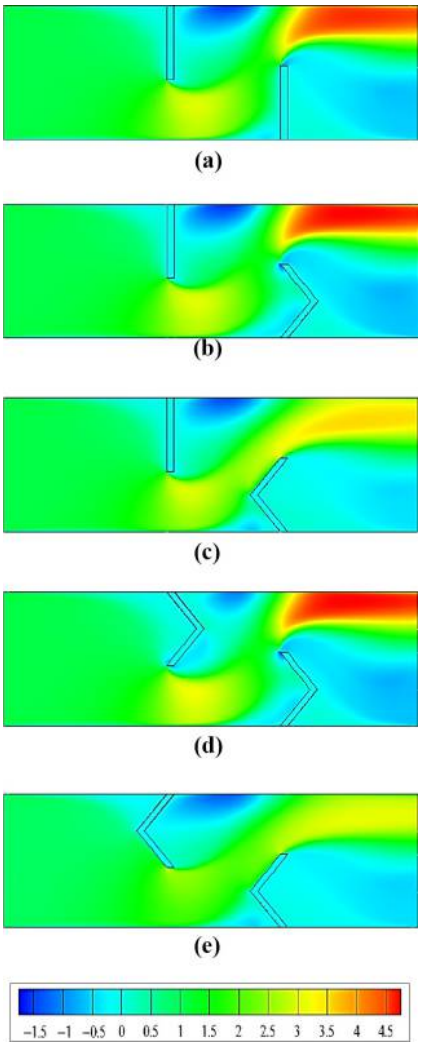

Figure 6.
Axial velocity contours in m/s for (a) FF-, (b) FVD-, (c) FVU-, (d) VVD- and (e) VVU-type obstacles at Re = 12,000

As for the transverse component of the velocity, it is interesting to note that for all the cases studied (FF, FVD, FVU, VVD, and VVU), negative velocity gradients are observed at the top of the hot upper channel wall-mounted left obstacle and positive velocity gradients at the top of the insulated lower wall-fixed right obstacle [Figure 7(a)-(e)].

The presence of the flat and/or V-shaped obstacles influences not only the velocity field but also the dynamic pressure distribution in the whole domain examined (Figure 8). Low and high pressure regions are associated to recirculation regions. The most intense is that occurring downstream of the right obstacle, near the heated upper wall of the channel, responsible for the high flow velocities observed at the exit, creating a negative velocity profile which introduces mass inside the channel through the outlet. The lower dynamic pressure values in the vicinity of each obstacle are due to the low velocities in that region, as

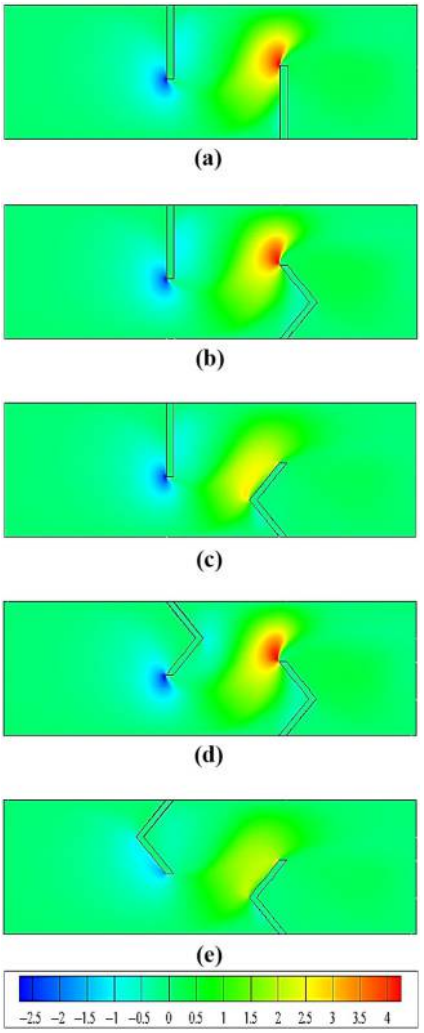

Figure 7.
Transverse velocity contours in m/s for (a) FF-, (b) FVD-, (c) FVU-, (d) VVD- and (e) VVU-type obstacles at Re = 12,000

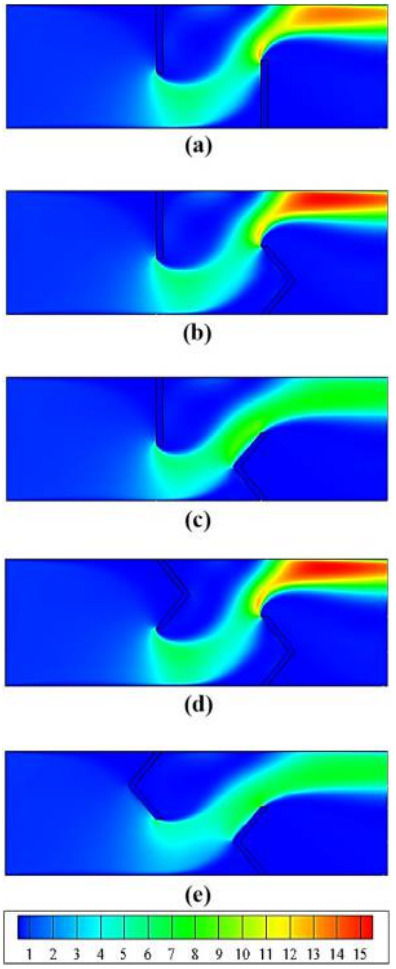

Figure 8.
Dynamic pressure contours in Pa for (a) FF-, (b) FVD-, (c) FVU-, (d) VVD- and (e) VVU-type obstacles at Re = 12,000

found and confirmed experimentally by Demartini *et al.* (2004). Similar to the results in Figure 6, in the FVU and VVU configurations, it is clear that the value of dynamic pressure has the lowest values by comparing with other cases.

Figure 9(a)-(e) depicts the contour plots of temperature in the entire region under study, for the cases FF, FVD, FVU, VVD and VVU, respectively. One can easily notice, on the figure, that the temperature changes significantly over the hot upper wall of the channel for all cases investigated.

Figure 10(a) and (b) shows the distribution of dimensionless axial velocity profiles in the sections starting from the tip of the obstacles to the opposite walls. Velocity measurements were performed for various obstacle configurations at Re = 12,000. Figure 10(a) shows computational results under the left obstacle at $x = 0.223$ m, while Figure 10(b) shows the results above the right obstacle at $x = 0.375$ m. In both stations, the airflow is accelerated due to the effect of cross-sectional reduction. The values of velocities for all the studied cases are higher than velocity inlet. In the case of simple obstacles (FF), the axial velocity is found to

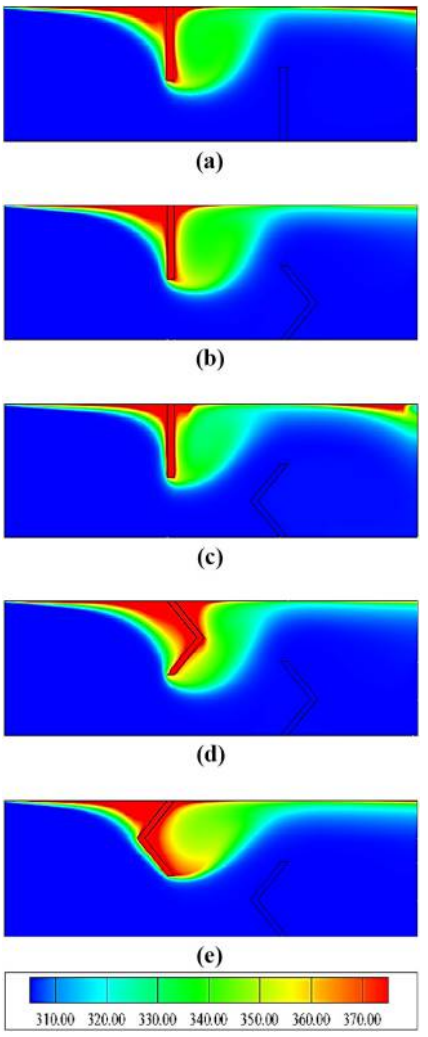

Figure 9.
Temperature contours in m/s for (a) FF-, (b) FVD-, (c) FVU-, (d) VVD- and (e) VVU-type obstacles at Re = 12,000

be highest by about 303.730 per cent compared to the inlet velocity [Figure 10(b)]. This value decreases in the VVU case by 3.097 per cent at $x = 0.375$ m. However, the axial velocity increases by 1.273, 7.816 and 9.709 per cent when the channel is equipped with FVU, FVD and VVD type obstacles, respectively, at the same station, and thus, the case of VVD type obstacles provides maximum axial velocity.

The dimensionless axial velocity profiles right after the first and second obstacles, at the two stations $x = 0.315$ m and $x = 0.525$ m from the entrance, are compared in Figure 11(a) and (b), respectively. The previous figures indicate that the change in the obstacle shape and disposition has a strong effect on the form of the axial velocity and on the recirculation length produced in the downstream region of the first obstacle [at $x = 0.315$ m in Figure 11(a)] and the second obstacle [at $x = 0.525$ m in Figure 11(b)].

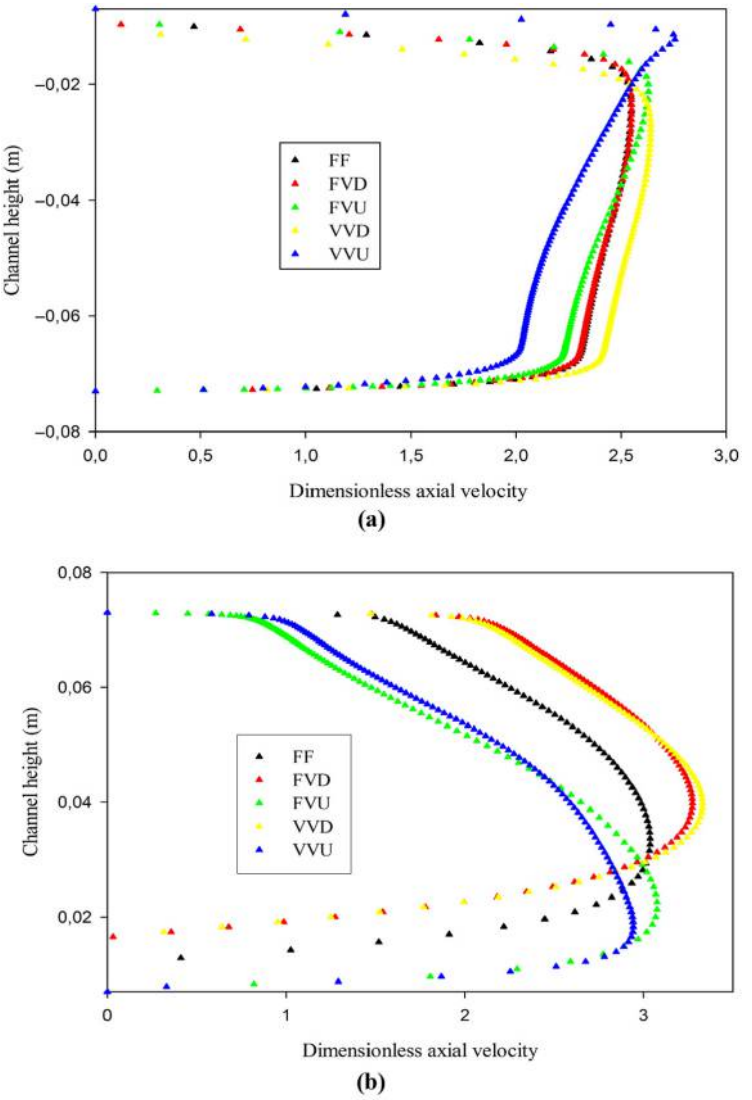

Notes: (a) Under the fin at x = 0.223 m; (b) above the baffle at x = 0.375 m for various obstacles at Re = 12,000

Figure 10.
Dimensionless axial velocity profiles

Recirculation cells, with very low velocities, are observed at the two positions. These cells are due to the flow separation. The flow is reversed and this causes its detachment near the two walls of the channel. The velocity profiles are oriented in the direction opposite to the flow. The hot fin fixed at the top surface of the channel has a velocity profile [at $x = 0.315$ m, in Figure 11(a)]; its dimensions are considerably larger than those of the baffle mounted on the insolated surface [at $x = 0.525$ m in Figure 11(b)].

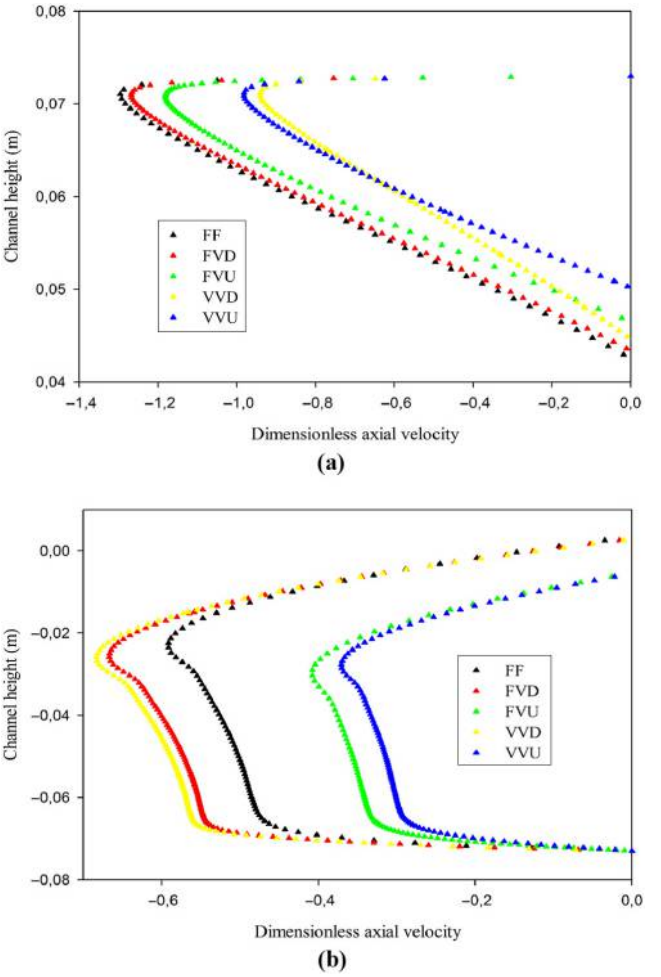

Figure 11.
Effect of obstacle geometry and disposition on the recirculation length behind (a) the fin at $x = 0.315$ m and (b) the baffle at $x = 0.525$ m for $Re = 12{,}000$

This has an impact on the reattachment lengths and on the dimensions of the recirculation zones of the five cases to be studied. For example, Figure 11(a) shows the effect of the fin reconfiguration and orientation on the counter rotating flow pattern behind the left obstacle, of which the maximum absolute value of axial velocity in the case of the simple baffles (or flat fin and flat baffle [FF]) is equal to 1.360 m/s, whereas in the cases of the FVD-, FVU-, VVD- and VVU-type obstacles, we find, respectively, maximum absolute values of axial velocity equal to 1.330 m/s, 1.239 m/s, 0.987 m/s, and 1.031 m/s differently say reductions of 2.205 per cent, 8.897 per cent, 27.426 per cent, and 24.191 per cent compared to the FF obstacles. The comparison of the recirculation length for various obstacles, in Figure 11(b), shows that the VVD-type obstacle case generates the longest vortex. At this station $x = 0.525$ m, the absolute value of the axial velocity for this VVD case reaches 0.716 m/s. This value decreases when the channel is fitted with obstacles in the FF, FVD, FVU and VVU models by 13.407, 2.374, 40.363 and 45.670 per cent, respectively.

4.2 Heat transfer and skin friction loss

Figure 12(a) and (b) shows, respectively, the variations in the normalized local (Nu_x/Nu_0) and average (Nu/Nu_0) Nusselt numbers, for different obstacle cases treated. Nu_0 is the Nusselt number for turbulent flow in a smooth channel at the same Reynolds number and is given by equation (28). The trends of (Nu_x/Nu_0) are similar for all obstacle forms and dispositions under study. The results obtained are found to be consistent with those reported by several authors who confirm that some recirculation zones appear locally; this corresponds to a more significant heat transfer (Nasiruddin and Siddiqui, 2007). The maximum Nu_x/Nu_0 is obtained for case of VVD-type obstacles, while the lowest one is for case of VVU-type obstacles. In addition, the increases in local Nusselt number values for using FF, FVD, FVU, VVD and VVU model obstacles, respectively, are about 61.797, 74.514, 76.831, 78.639 and 55.611 times over the smooth rectangular channel, as shown in Figure 12(a). In Figure 12(b), the average Nusselt number ratio tends to increase with the rise of Reynolds number from

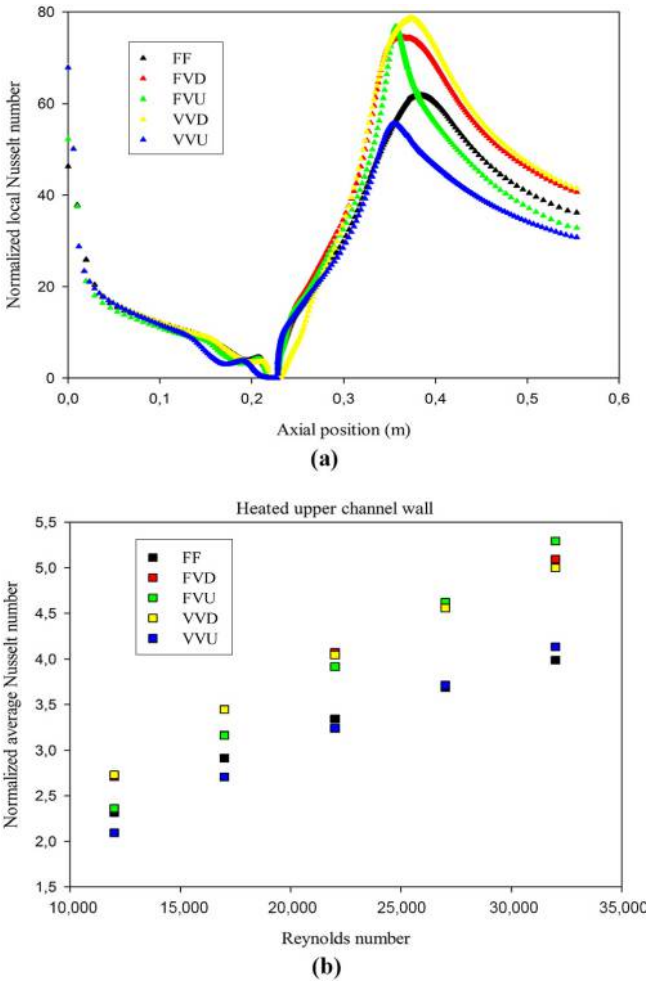

Figure 12. Dimensionless profiles of normalized (a) local and (b) average Nusselt numbers for various cases treated

12,000 to 32,000 for all deflectors. Over range studies, the *Nu* values for FF-, FVD-, FVU-, VVD- and VVU-type obstacles are in the range of 231.360-398.936, 270.983-509.684, 235.987-529.044, 272.991-500.133 and 209.585-413.557 per cent above the smooth air channel with no obstacle, respectively. This indicates that the FVU gives higher heat transfer than the FF, FVD, VVD and VVU with values of 24.593, 3.659, 5.464 and 21.829 per cent, respectively, at the highest value of Reynolds number ($Re = 32{,}000$).

Figure 13(a) shows the numerical results of normalized local skin friction coefficient distributions (C_f/f_0) for configurations FF, FVD, FVU, VVD and VVU. Here, f_0 is the friction factor in a smooth air channel for the turbulent flow at the same Reynolds number, and it can be presented as shown, above, in equation (29). The lowest C_f value is found on the side upstream of the left obstacle, but the highest value is encountered on the side in front of the right obstacle, for all the instances under consideration. The use of VVD-obstacles provides a maximum C_f value, while the VVU obstacle gives a minimum for almost locations. For the

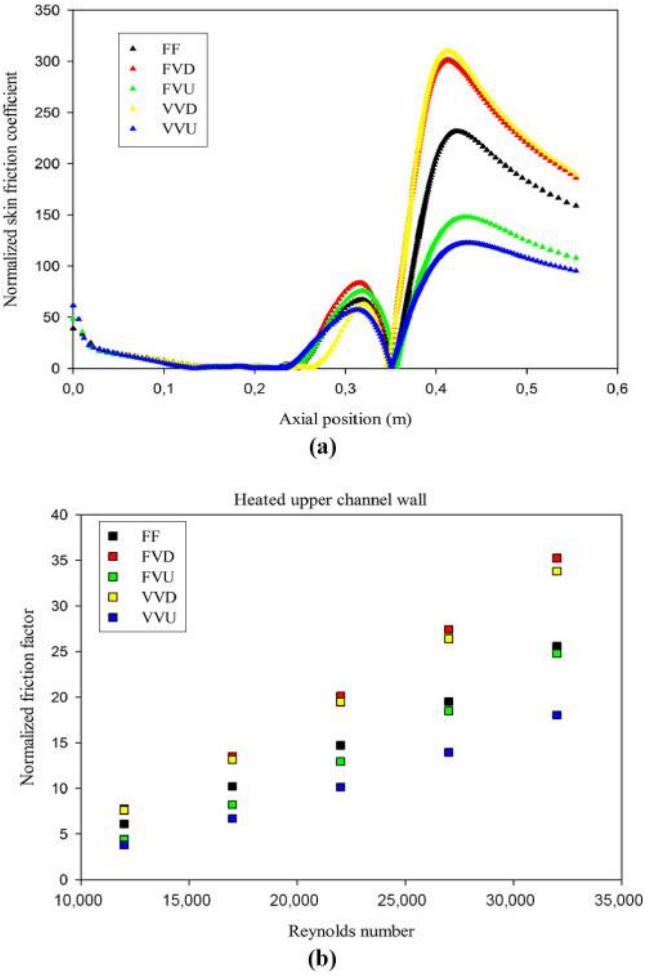

Figure 13.
Dimensionless profiles of normalized (a) local and (b) average skin friction coefficients for various cases treated

VVU case, the V-upstream obstacle is pointed toward the upstream side; therefore, it causes less distortion of the flow, especially at lower *Re* and θ values (*Re* = 12,000, and θ = 45°), whereas for VVD case, the V-downstream obstacle is toward the downstream side, which causes significantly large flow distortion, where the effect of pressure loss is very significant. For the lowest value of *Re* number, the increases in C_f/f_0 for the FF, FVD, FVU, VVD and VVU obstacles are, respectively, about 231.744, 301.083, 147.949, 309.729 and 122.665 times above the smooth rectangular air channel with no fin and baffle. This suggests that the use of the VVU obstacles can help to reduce the friction loss considerably. Importantly, the channel with VVU obstacles at *Re* = 12,000 shows lower skin friction loss than the one with FF, FVD, FVU and VVD obstacles around 88.924, 145.451, 20.612 and 152.499 per cent, respectively.

The variation of normalized friction factor (f/f_0) is also presented in Figure 13 [see Figure 13(b)] which shows that the (f/f_0) increases with the rise of Reynolds number. The *f* values in the air channel with FF, FVD, FVU, VVD and VVU obstacles are, respectively, 6.103-25.606, 7.772-35.227, 4.421-24.787, 7.598-33.788 and 3.807-18.043 times higher than those in the smooth air channel with no obstacle. As the figure, the FVD or VVD cases perform greater friction factor than the FVU or VVU cases. The reason of this may be that the V-downstream can produce stronger impinging flow than the V-upstream. In a comparison with the simple obstacles (FF case), the *f* value increases in the cases of FVD and VVD by 37.573 and 31.952 per cent, respectively, at the highest value of Reynolds number (*Re* = 32,000). However, the *f* value decreases by 3.199 and 29.535 per cent when the obstacle models are FVU and VVU, respectively, at the same Reynolds number, which indicates that the FVU- and VVU-type obstacle cases are more advantageous than the others.

4.3 Performance evaluation

Figure 14 shows the variations of TEF as a function of the Reynolds number at various investigated cases. In the figure, the TEF value tends to increase with augmenting the *Re* number. The channel containing the flat fin and the 45° FVU provides the highest TEF value, while that with FF yields the lowest one. It is found that the TEF values are 1.273-1.368, 1.377-1.573, 1.444-1.833, 1.398-1.565 and 1.348-1.592 for FF, FVD, FVU, VVD and VVU, respectively, depending on the *Re* values. In all situations, the TEF was found to be

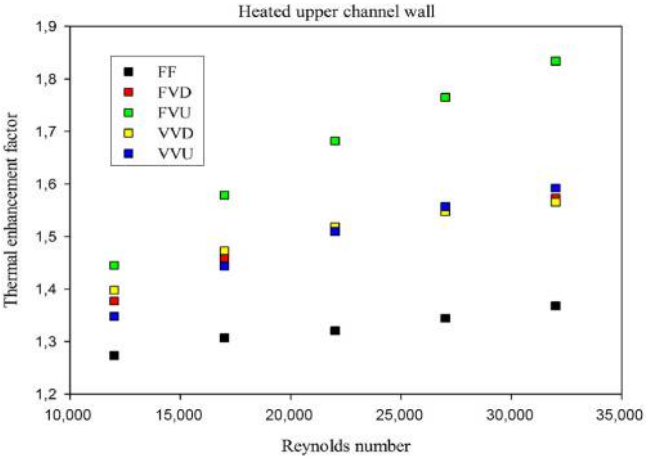

Figure 14. Thermal enhancement factor for various obstacles

much larger than unity; its maximum value was around 1.833 for FVU and Re = 32,000. This value of TEF is decreased by 25.397, 14.210, 14.651 and 13.193 per cent in the case of FF-, FVD-, VVD- and VVU-type obstacles at the same Re number, respectively. Therefore, the FVU may be considered as the best geometrical configuration when using the obstacles to augment the heat transfer in the channel.

5. Conclusion

CFD analysis for turbulent flow, forced-convection and thermal enhancement efficiency in a high-performance rectangular cross section channel with hot top and insulated bottom wall-mounted staggered solid-type obstacles were performed using the commercial CFD software FLUENT software. Two transverse, solid-type obstacles, having different shapes, i.e. flat rectangular and V-shaped, were introduced within the channel; they were arranged on the top and bottom surfaces in a periodically staggered manner to force vortices to have a substantial influence on the turbulence intensity of the flow, thus causing a larger heat transfer enhancement in the entire domain under investigation. Air is the test fluid with the flow rate in terms of Reynolds numbers ranging from 12,000 to 32,000. The governing flow equations (i.e. continuity, momentum and energy equations) used to simulate the incompressible steady airflow and convective heat transfer in the given computational domain were discretized using the FVM. The most important conclusions that can be drawn from this study are as follows:

- Important deformations and large recirculation regions were observed in the flow field.
- The hot fin fixed at the top surface of the channel has a velocity profile; its dimensions are considerably larger than those of the baffle mounted on the insolated surface. This has an impact on the reattachment lengths and on the dimensions of the recirculation zones of the five cases to be studied. The recycling cells are situated by the right sides of the obstacles and their heights are nearly equal to the magnitude of the flow blockage by the obstacle; it is equal to 0.08 m for the configuration under study.
- The higher temperature gradient can be observed in the top flow region where the air impinges the hot upper channel wall, while the lower one can be found in the area opposite the fin tip or at the bottom flow regime, in all cases examined.
- The largest value of the axial variations of the Nusselt number and skin friction coefficient is found in the region facing the baffle, while the smallest value is in the region near the fin, for all cases.
- Over range studies, the average Nusselt number values for FF-, FVD-, FVU-, VVD- and VVU-type obstacles are in the range of 231.360-398.936, 270.983-509.684, 235.987-529.044, 272.991-500.133 and 209.585-413.557 per cent above the smooth air channel with no obstacle, respectively.
- Result analysis indicates that the FVU-type obstacles gives higher heat transfer than the FF-, FVD-, VVD- and VVU-type obstacles with values of 24.593 per cent, 3.659, 5.464 and 21.829 per cent, respectively, at the highest value of Reynolds number.
- The friction factor values in the air channel with FF-, FVD- FVU-, VVD- and VVU-type obstacles are, respectively, 6.103-25.606, 7.772-35.227, 4.421-24.787, 7.598-33.788 and 3.807-18.043 times higher than those in the smooth air channel with no obstacle, depending on the Re values.

- In a comparison with the simple obstacles (FF type-obstacle case), the friction factor value increases in the cases of FVD and VVD by 37.573 and 31.952 per cent, respectively, at the highest value of Reynolds number. However, the friction factor value decreases by 3.199 and 29.535 per cent when the obstacle models are FVU and VVU, respectively, at the same Reynolds number, which indicates that the FVU- and VVU-type obstacle cases are more advantageous than the others.
- The channel containing the flat fin and the 45° FVU provides the highest TEF value, while that with FF yields the lowest one. In all situations, the TEF was found to be much larger than unity; its maximum value was around 1.833 for FVU and Re = 32,000. Therefore, the FVU may be considered as the best geometrical configuration when using the obstacles to enhance the heat transfer inside the channel.
- Future work will involve more complex geometries and using nanofluids to assess the optimum conditions for heat transfer enhancements.

References

Aharwal, K.R., Gandhi, B.K. and Saini, J.S. (2008), "Experimental investigation on heat-transfer enhancement due to a gap in an inclined continuous rib arrangement in a rectangular duct of solar air heater", *Renewable Energy*, Vol. 33 No. 4, pp. 585-596.

Ahmed, S.E., Rashad, A.M. and Gorla, R.S.R. (2013), "Natural convection in triangular enclosures filled with Nanofluid saturated porous media", *Journal of Thermophysics and Heat Transfer*, Vol. 27 No. 4, pp. 700-706.

Armaghani, T., Kasaeipoor, A., Izadi, M. and Pop, I. (2018), "MHD natural convection and entropy analysis of a nanofluid inside T-shaped baffled enclosure", *International Journal of Numerical Methods for Heat and Fluid Flow*, available at: https://doi.org/10.1108/HFF-02-2018-0041

Behseresht, A., Noghrehabadi, A. and Ghalambaz, M. (2014), "Natural-convection heat and mass transfer from a vertical cone in porous media filled with nanofluids using the practical ranges of nanofluids thermo-physical properties", *Chemical Engineering Research and Design*, Vol. 92 No. 3, pp. 447-452.

Ben Slama, R. (2007), "The air solar collectors: comparative study, introduction of baffles to favor the heat transfer", *Solar Energy*, Vol. 81, pp. 139-149.

Berner, C., Durst, F. and McEligot, D.M. (1984), "Flow around baffles", *Journal of Heat Transfer*, Vol. 106 No. 4, pp. 743-749.

Demartini, L.C., Vielmo, H.A. and Möller, Q.V. (2004), "Numeric and experimental analysis of turbulent flow through a channel with baffle plates", *Journal of the Brazilian Society of Mechanical Sciences and Engineering*, Vol. 26 No. 2, pp. 153-159.

Dittus, F.W. and Boelter, L.M.K. (1930), "Heat transfer in automobile radiators of tubular type", *University of CA Publications in Engineering*, Vol. 2, University of CA Press, Berkeley, CA, available at: https://doi.org/10.1016/0735-1933(85)90003-X

Dutta, P. and Hossain, A. (2005), "Internal cooling augmentation in rectangular channel using two inclined baffles", *International Journal of Heat and Fluid Flow*, Vol. 26 No. 2, pp. 223-232.

EL-Kabeir, S.M.M., Rashad, A.M. and Gorla, R.S.R. (2007), "Unsteady MHD combined convection over a moving vertical sheet in a fluid saturated porous medium with uniform surface heat flux", *Mathematical and Computer Modelling*, Vol. 46 Nos 3/4, pp. 384-397.

Endres, L.A.M. and Möller, S.V. (2001), "On the fluctuating wall pressure field in tube banks", *Nuclear Engineering Design*, Vol. 203 No. 1, pp. 13-26.

Fiebig, M., Kallweit, P., Mitra, N. and Tiggel, B.S. (1991), "Heat transfer enhancement and drag by longitudinal vortex generators in channel flow", *Journal of Experimental Thermal Fluid Science*, Vol. 4 No. 1, pp. 103-114.

Ghalambaz, M. and Noghrehabadi, M. (2014), "Effects of heat generation/absorption on natural convection of nanofluids over the vertical plate embedded in a porous medium using drift-flux model", *Journal of Computational and Applied Research in Mechanical Engineering*, Vol. 3, pp. 113-123.

Ghalambaz, M., Noghrehabadi, A. and Ghanbarzadeh, A. (2014a), "Effects of variable viscosity and thermal conductivity on natural-convection of nanofluids past a vertical plate in porous media", *Journal of Mechanics*, Vol. 30 No. 3, pp. 265-275.

Ghalambaz, M., Noghrehabadi, A.R. and Ghanbarzadeh, A. (2014b), "Natural convection of nanofluids over a convectively heated vertical plate embedded in a porous medium", *Brazilian Journal of Chemical Engineering*, Vol. 31 No. 2, pp. 413-427.

Habib, M.A., Attya, A.E. and McEligot, D.M. (1988), "Calculation of turbulent flow and heat transfer in channels with streamwise-periodic flow", *Journal of Turbomachinery*, Vol. 110 No. 3, pp. 405-411.

Han, J.C. and Park, J.S. (1988), "Developing heat transfer in a rectangular channel with rib turbulators", *ASME Journal of Heat Transfer*, Vol. 31 No. 1, pp. 183-195.

Han, J.C., Park, J.S. and Lei, C.K. (1985), "Heat transfer enhancement in channels with turbulence promoters", *ASME Journal of Engineering for Gas Turbines and Power*, Vol. 107 No. 3, pp. 628-635.

Ho, M.C. and Ramaswamy, B. (1995), "Use of baffles in cavity flow for the suppression of thermal oscillations under microgravity", *International Journal of Numerical Methods for Heat and Fluid Flow*, Vol. 5 No. 2, pp. 141-173.

Hwang, C.B. and Lin, C.A. (1999), "A low Reynolds number two-equation k_{θ}-ε_{θ} model to predict thermal fields", *International Journal of Heat and Mass Transfer*, Vol. 42 No. 17, pp. 3217-3230.

Jedsadaratanachai, W. and Boonloi, A. (2014), "Effects of blockage ratio and pitch ratio on thermal performance in a square channel with 30° double V-baffles", *Case Studies in Thermal Engineering*, Vol. 4, pp. 118-128.

Kahalerras, H. and Targui, N. (2008), "Numerical analysis of heat transfer enhancement in a double pipe heat exchanger with porous fins", *International Journal of Numerical Methods for Heat and Fluid Flow*, Vol. 18 No. 5, pp. 593-617.

Karwa, R.K. (2003), "Experimental studies of augmented heat transfer and friction in symmetrically heated rectangular ducts with ribs on heated wall in transverse, inclined, v-continuous and v-discrete pattern", *International Communication in Heat and Mass Transfer*, Vol. 30 No. 2, pp. 241-250.

Kelkar, K.M. and Patankar, S.V. (1987), "Numerical prediction of flow and heat transfer in a parallel plate channel with staggered fins", *Journal of Heat Transfer*, Vol. 109 No. 1, pp. 25-30.

Ko, K.H. and Anand, N.K. (2003), "Use of porous baffles to enhance heat transfer in a rectangular channel", *International Journal of Heat and Mass Transfer*, Vol. 46 No. 22, pp. 4191-4199.

Launder, B.E. and Spalding, D.B. (1974), "The numerical computation of turbulent flows", *Computer Methods Applied Mechanics Engineering*, Vol. 3 No. 2, pp. 269-289.

Lei, Y.G., He, Y.L., Li, R. and Gao, Y.F. (2008), "Effects of baffle inclination angle on flow and heat transfer of a heat exchanger with helical baffles", *Chemical Engineering Processing*, Vol. 47 No. 12, pp. 2336-2345.

Leonard, B.P. and Mokhtari, S. (1990), "ULTRA-SHARP nonoscillatory convection schemes for high-speed steady multidimensional flow", NASA TM 1-2568, NASA Lewis Research Center.

Liou, T.M. and Wang, W.B. (1995), "Laser holographic-interferometry study of developing heat-transfer in a duct with a detached rib array", *International Journal of Heat Mass Transfer*, Vol. 38 No. 1, pp. 91-100.

Liu, H. and Wang, J. (2011), "Numerical investigation on synthetical performances of fluid flow and heat transfer of semiattached rib-channels", *International Journal of Heat and Mass Transfer*, Vol. 54 Nos 1/3, pp. 575-583.

Mansour, M.A., Ahmed, S.E. and Rashad, A.M. (2016), "MHD natural convection in a square enclosure using nanofluid with the influence of thermal boundary conditions", *Journal of Applied Fluid Mechanics*, Vol. 9 No. 5, pp. 2515-2525.

Maurer, M., Jens, V.W. and Gritisch, M. (2007), "An experimental and numerical study of heat transfer and pressure losses of V and W shaped ribs at high Reynolds number", *Proceedings of the ASME Turbo Expo*, Vol. 4, pp. 219-228.

Mehryan, S.A.M., Ghalambaz, M. and Izadi, M. (2018), "Conjugate natural convection of nanofluids inside an enclosure filled by three layers of solid, porous medium and free nanofluid using Buongiorno's and local thermal non-equilibrium models", *Journal of Thermal Analysis and Calorimetry*, available at: https://doi.org/10.1007/s10973-018-7380-y

Nasiruddin and Siddiqui, M.H.K. (2007), "Heat transfer augmentation in a heat exchanger tube using a baffle", *International Journal of Heat and Fluid Flow*, Vol. 28, pp. 318-328.

Nguyen, M.T., Aly, A.M. and Lee, S.W. (2017), "A numerical study on unsteady natural/mixed convection in a cavity with fixed and moving rigid bodies using the ISPH method", *International Journal of Numerical Methods for Heat and Fluid Flow*, available at: https://doi.org/10.1108/HFF-02-2017-0058

Noghrehabadi, A.R., Saffarian, M.R., Pourrajab, R. and Ghalambaz, M. (2013), "Entropy analysis for nanofluid flow over a stretching sheet in the presence of heat generation/absorption and partial slip", *Journal of Mechanical Science and Technology*, Vol. 27 No. 3, pp. 927-937.

Patankar, S.V. (1980), *Numerical Heat Transfer and Fluid Flow*, McGraw-Hill, New York, NY.

Petukhov, B. (1970), "Heat transfer and friction in turbulent pipe flow with variable physical properties", *Advances in Heat Transfer*, Vol. 6, pp. 503-564.

Pirouz, M.M., Farhadi, M., Sedighi, K., Nemati, H. and Fattahi, E. (2011), "Lattice Boltzmann simulation of conjugate heat transfer in a rectangular channel with wall-mounted obstacles", *Scientia Iranica B*, Vol. 18 No. 2, pp. 213-221.

Rashad, A.M. (2008), "Influence of radiation on MHD free convection from a vertical flat plate embedded in porous media with thermophoretic deposition of particles", *Communications in Nonlinear Science and Numerical Simulation*, Vol. 13 No. 10, pp. 2213-2222.

Rashad, A.M., EL-Hakiem, M.A. and Abdou, M.M.M. (2011), "Natural convection boundary layer of a non-Newtonian fluid about a permeable vertical cone embedded in a porous medium saturated with a nanofluid", *Computers and Mathematics with Applications*, Vol. 62 No. 8, pp. 3140-3151.

Sahel, D., Ameur, H., Benzeguir, R. and Kamla, Y. (2016), "Enhancement of heat transfer in a rectangular channel with perforated baffles", *Applied Thermal Engineering*, Vol. 101, pp. 156-164.

Sheremet, M. and Chinnasamy, S. (2018), "Convective-radiative heat transfer in a cavity filled with a nanofluid under the effect of a nonuniformly heated plate", *International Journal of Numerical Methods for Heat and Fluid Flow*, available at: https://doi.org/10.1108/HFF-06-2017-0255

Shuja, S.Z., Yilbas, B.S. and Kassas, M. (2010), "Entropy generation in a square cavity", *International Journal of Numerical Methods for Heat and Fluid Flow*, Vol. 20 No. 3, pp. 332-347.

Sripattanapipat, S. and Promvonge, P. (2009), "Numerical analysis of laminar heat transfer in a channel with diamond-shaped baffles", *International Communication in Heat and Mass Transfer*, Vol. 36 No. 1, pp. 32-38.

Tahmasebi, A., Mahdavi, M. and Ghalambaz, M. (2018), "Local thermal nonequilibrium conjugate natural convection heat transfer of nanofluids in a cavity partially filled with porous media using Buongiorno's model", *Numerical Heat Transfer, Part A: Applications*, Vol. 73 No. 4, pp. 254-276.

Tamna, S., Skullong, S., Thianpong, C. and Promvonge, P. (2014), "Heat transfer behaviors in a solar air heater channel with multiple V-baffle vortex generators", *Solar Energy*, Vol. 110, pp. 720-735.

Tanda, G. (2011), "Effect of rib spacing on heat transfer and friction in a rectangular channel with 45° angled rib turbulators on one/two walls", *International Journal of Heat and Mass Transfer*, Vol. 54 Nos 5/6, pp. 1081-1090.

Taslim, M.E. and Li, T. (1996), "Experimental heat transfer and friction in channels roughened with angled, V-shaped, and discrete ribs on two opposite walls", *Journal of Turbomachinery*, Vol. 118 No. 1, pp. 20-28.

Ünalan, S., Akansu, S.O. and Konca, A. (2007), "Investigation of heat transfer and pressure drop for various obstacles in a rectangular-sectioned 90° bend", *International Journal of Numerical Methods for Heat and Fluid Flow*, Vol. 17 No. 5, pp. 494-511.

Verma, S.K. and Prasad, B.N. (2000), "Investigation for the optimal thermohydraulic performance of artificially roughened solar air heaters", *Renewable Energy*, Vol. 20 No. 1, pp. 19-36.

Won, S.Y., Burgess, N.K., Peddicord, S. and Ligrani, P.M. (2004), "Spatially resolved surface heat transfer for parallel rib turbulators with 45 deg. orientations including test surface conduction analysis", *Journal of Heat Transfer*, Vol. 126 No. 2, pp. 193-201.

Yang, M.-H., Yeh, R.-H. and Hwang, J.-J. (2012), "Forced convection in a channel with transverse fins", *International Journal of Numerical Methods for Heat and Fluid Flow*, Vol. 22 No. 3, pp. 306-322.

Yongsiri, K., Eiamsa-ard, P., Wongcharee, K. and Eiamsa-ard, S. (2014), "Augmented heat transfer in a turbulent channel flow with inclined detached-ribs", *Case Studies in Thermal Engineering*, Vol. 3, pp. 1-10.

Zhou, G. and Ye, Q. (2012), "Experimental investigations of thermal and flow characteristics of curved trapezoidal winglet type vortex generators", *Applied Thermal Engineering*, Vol. 37, pp. 241-248.

Corresponding author
Younes Menni can be contacted at: menniyounes.cfd@gmail.com